



**Quantum wetting transition in the one-dimensional transverse-field Ising model with random bonds**Kun Hu  and Xintian Wu\**Department of Physics, Beijing Normal University, Beijing, 100875, China* (Received 14 July 2021; revised 21 September 2021; accepted 19 October 2021; published 27 October 2021)

The quantum wetting transition in the one-dimensional transverse-field Ising model with random bonds is studied. Opposite boundary fields are applied at the two ends of the Ising chain. The interface between two domains with oppositely oriented magnetization is localized near the boundary or in the middle of the chain. The wetting transition refers to the phase transition of localization and delocalization of the interface. The tuning parameter  $h_L$  is the boundary field at one end, e.g., the left end. At the transition point  $h_L = h_w$ , the wetting transition occurs. First, we study the wetting transition with one defect bond. It is a first-order transition, and the interface jumps from the left end of the chain to the defect bond at the transition point. Second, we study the wetting transition with two defect bonds and find that the weaker defect bond dominates the phase transition. The wetting transition is still first order, and the interface is localized at the left end of the chain or at the weaker defect bond. Lastly, the random bond case is studied. The random bonds have a rectangular distribution. The wetting transition is still first order. The finite-size effects are studied. The statistics of the transition points and the energy gaps are obtained. We study lattices with sizes  $N = 100, 150, 200, 250, 300,$  and  $350$ . The deviation of the phase transition points  $h_w$  does not decrease as the lattice size increases. It is argued that the transition point is sample dependent, i.e., the variation in the transition point  $h_w$  does not approach zero, even at the thermodynamic limit.

DOI: [10.1103/PhysRevB.104.134430](https://doi.org/10.1103/PhysRevB.104.134430)**I. INTRODUCTION**

The influence of quenched disorder on the phase transition has been an interesting topic in theoretical and experimental physics [1]. The quantum phase transition has become an important topic in recent years due to the discovery of many new materials and the development of cold atom technology [2–5]. In this paper we study a quantum phase transition with disorder, the wetting transition, in the one-dimensional transverse-field Ising model with random bonds.

The one-dimensional transverse-field Ising model with random bonds is famous for its Griffiths-McCoy singularity, where several thermodynamic observables, including the average susceptibility, actually diverge in a finite region of the disordered phase rather than only at the critical point [6–10]. The Griffiths-McCoy singularity was first discovered in the McCoy-Wu model, which is the classical counterpart of the transverse-field Ising model with random bonds [11–13]. Some quantum spin models in the  $d$  dimension can be mapped to classical spin models in the  $d + 1$  dimension [14]. The wetting transition in the McCoy-Wu model has been studied recently [15]. It is found that the phase transition is still first order, although disorder is present. Generally, disorder can alter the order of the phase transition. It is shown rigorously that the quenched randomness suppresses the first-order phase transitions in the two-dimensional random-field Ising model, random-bond Potts model, and spin glasses [16]. Therefore,

the first-order phase transition in disordered systems is an interesting topic.

Wetting phenomena have attracted enormous theoretical and experimental attention [17,18]. Such phenomena occur, e.g., in binary liquid mixtures below the consolution point, where one phase is generally adsorbed on the container wall and may wet its surface when phases coexist. The wetting transition can be viewed as delocalization of the interface between the adsorbed phase and the bulk phase of the mixture. Far from the bulk critical temperature  $T_c$ , the interface is localized near the wall, but at some finite temperature less than  $T_c$ , the thickness of the wetting layer diverges. Due to the well-known correspondence between Ising ferromagnets and lattice-gas models of gas-fluid systems, the wetting transition can be studied using Ising models with surface fields [19]. In the ordered state a continuous wetting transition is observed in the two-dimensional Ising model [20–24]. For an Ising ferromagnet with positive magnetization in the bulk, at zero bulk field, a negative boundary field  $H_1$  at the wall may stabilize a domain with oppositely oriented magnetization at the surface.

For the one-dimensional transverse-field Ising model, one can realize the quantum wetting transition by applying opposite surface fields on the two open ends [15]. The two boundary fields are in opposite directions, so there is an interface between the two domains with oppositely oriented magnetization. The interface is localized either at one boundary or in the middle. The wetting transition is the transition of the interface. Tuning the surface fields, the interface's position changes drastically at the phase transition point. In the clean system, i.e., with uniform bonds, first-order and second-order wetting transitions are shown [15].

\*wuxt@bnu.edu.cn

In this paper we study the wetting transition in the one-dimensional transverse-field Ising model with random bonds. To understand the phase transition mechanism, we first studied the phase transition with one bond defect and two bond defects. Then we studied the random bond case, where the random bonds have a rectangular distribution. The second-order transition in the clean system is absent due to the disorder of the lattice. Instead, the phase transition is first order. The finite-size effects are studied. This model shows interesting finite-size effects. For a finite-size sample, e.g., a 200-site-long Ising chain, there may be no singular behavior, but adding another 200 sites to it may lead to singular behaviors. Alternatively, a 200-site-long Ising chain shows a first-order phase transition at a specific surface field, and adding another 200 sites leads to a first-order phase transition at a different surface field, replacing the original phase transition. In other words, when the systems are lengthened, the phase transition point may move.

The statistical properties of the energy gap and transition point for  $N = 100, 150, 200, 250, 300, 350$  samples are also obtained. For each size, 20000 samples are calculated. It is found that the distribution width of the surface field at the transition point does not decrease with the size.

In our numerical calculations, the lattice length is finite, the ‘‘phase transition’’ refers to pseudosingularity in finite-size systems since the phase transition occurs at the limit of the thermodynamic limit where the system size approaches infinitely large.

By extrapolating the results on the finite-size lattices, we conclude that the wetting transition point is sample dependent in the limit of an infinitely large lattice, i.e., the surface field at the transition point depends on the sample, even at the thermodynamic limit. To our knowledge, in all previously studied disordered systems, the phase transition temperatures converge to a limit as the system size approaches infinity (see examples in Refs. [25–27]). We discuss the reason for this unusual effect in the summary.

This paper is arranged as follows. In Sec. II we present the model and the solving method. In Sec. III we analytically solve the phase transition with one defect. In Sec. IV we numerically solve the phase transition with two defects. In Sec. V we show the finite-size effects in random-bond systems. In Sec. VI we present the results of the phase transition with random bonds. Section VII includes a summary.

## II. THE MODEL AND THE SOLVING METHOD

We consider the one-dimensional transverse-field Ising chain with boundary fields:

$$H = H_0 - h_L \sigma_1^{(1)} - h_R \sigma_N^{(1)}, \quad (1)$$

where

$$H_0 = - \sum_{i=1}^{i=N-1} K_i \sigma_i^{(1)} \sigma_{i+1}^{(1)} - g \sum_{i=1}^{i=N} \sigma_i^{(3)}, \quad (2)$$

$\sigma_i^{(1)}$  and  $\sigma_i^{(3)}$  are Pauli matrices, and  $h_L$  and  $h_R$  are the left and right boundary longitudinal fields, respectively. The interaction  $K_i$  is an independent random variable with distribution  $P(K)$ . The lattice size is  $N$ . Following the well-known

theories [28–31], we transform the diagonalization problem to an effective Hamiltonian by appending one additional spin to the left and right sides. The corresponding Hamiltonian is given by

$$H_e = H_0 - |h_L| \sigma_0^{(1)} \sigma_1^{(1)} - |h_R| \sigma_N^{(1)} \sigma_{N+1}^{(1)}. \quad (3)$$

Because  $\sigma_0^{(1)}, \sigma_{N+1}^{(1)}$  are free from the transverse field, both  $\sigma_0^{(1)}$  and  $\sigma_{N+1}^{(1)}$  commute with the Hamiltonian. Hence, they can be diagonalized simultaneously. The Hilbert space can be divided into four sectors, which we label  $(1, 1)$ ,  $(1, -1)$ ,  $(-1, 1)$ , and  $(-1, -1)$ , where  $(s_0, s_{N+1})$  are eigenvalues of  $\sigma_0^{(1)}$  and  $\sigma_{N+1}^{(1)}$ . The restriction of  $H_e$  to the four sectors gives rise to the Hamiltonian  $H$  with four cases of different signs of  $h_L, h_R$  [28]. For example, the restriction of  $H_e$  to sector  $(1, -1)$  gives rise to the Hamiltonian  $H$  with  $h_L > 0, h_R < 0$ . The first-order and second-order phase transitions occur in the region  $h_L h_R < 0$ . Therefore, we investigate case of  $h_L > 0, h_R < 0$  and the sector  $(1, -1)$ . The case  $h_L < 0, h_R > 0$  can be obtained with symmetry. To compute the spectrum of the Hamiltonian Eq. (3), we perform the Jordan-Wigner transformation and define fermionic operators

$$c_i^\dagger = (-1)^i \prod_{j=0}^{i-1} \sigma_j^{(3)} \sigma_i^+, \quad (4)$$

where  $\sigma^\pm = (\sigma^{(1)} \pm i\sigma^{(2)})/2$  ( $i$  is the imaginary unit). The Hamiltonian becomes

$$H_e = -gN + \sum_{i,j=0}^{N+1} \left( c_i^\dagger \mathbf{A}_{ij} c_j + \frac{1}{2} c_i^\dagger \mathbf{B}_{ij} c_j^\dagger - \frac{1}{2} c_i \mathbf{B}_{ij} c_j \right), \quad (5)$$

where  $\mathbf{A}$  and  $\mathbf{B}$  are symmetric and antisymmetric matrices, respectively. For clarity, here, we write the matrix elements explicitly for  $N = 3$  in the following:

$$\mathbf{A} = \begin{pmatrix} 0 & -|h_L| & 0 & 0 & 0 \\ -|h_L| & -2g & -K_1 & 0 & 0 \\ 0 & -K_1 & -2g & -K_2 & 0 \\ 0 & 0 & -K_2 & -2g & -|h_R| \\ 0 & 0 & 0 & -|h_R| & 0 \end{pmatrix}, \quad (6)$$

$$\mathbf{B} = \begin{pmatrix} 0 & -|h_L| & 0 & 0 & 0 \\ |h_L| & 0 & -K_1 & 0 & 0 \\ 0 & K_1 & 0 & -K_2 & 0 \\ 0 & 0 & K_2 & 0 & -|h_R| \\ 0 & 0 & 0 & |h_R| & 0 \end{pmatrix}. \quad (7)$$

We perform a Bogoliubov transformation by introducing new canonical fermionic variables [32]

$$\eta_k = g_{k,i} c_i + h_{k,i} c_i^\dagger. \quad (8)$$

By using these variables, the Hamiltonian can be diagonalized. The coefficients  $g_{k,i}$  and  $h_{k,i}$  satisfy the following equations:

$$g_{ki} = \frac{\phi_{k,i} + \psi_{k,i}}{2}, \quad h_{ki} = \frac{\phi_{k,i} - \psi_{k,i}}{2}, \quad (9)$$

where  $\psi_k$  is the eigenvector of the matrix

$$\mathbf{C} \equiv (\mathbf{A} + \mathbf{B})(\mathbf{A} - \mathbf{B}), \quad \mathbf{C}\psi_k = \varepsilon_k^2 \psi_k, \quad (10)$$

and

$$\phi_k = (\mathbf{A} - \mathbf{B})\psi_k/\varepsilon_k. \quad (11)$$

In the above equation,  $\varepsilon_k \neq 0$ . For the convenience of the readers, we write the matrix  $\mathbf{C}$ 's elements explicitly for  $N = 3$ :

$$\mathbf{C} = 4 \begin{pmatrix} h_L^2 & g|h_L| & 0 & 0 & 0 \\ g|h_L| & K_1^2 + g^2 & gK_1 & 0 & 0 \\ 0 & gK_1 & K_2^2 + g^2 & gK_2 & 0 \\ 0 & 0 & gK_2 & |h_R|^2 + g^2 & 0 \\ 0 & 0 & 0 & 0 & 0 \end{pmatrix}. \quad (12)$$

It is clear that there is a zero eigenvalue  $\varepsilon_0 = 0$  for  $\mathbf{C}$ . This mode is treated in Ref. [28]. The spectrum is doubly degenerate due to this zero mode. This degeneracy is the consequence of the  $Z_2$  global symmetry of the Hamiltonian  $H_e$ . The zero mode is not related to the spectrum of the Hamilton  $H$ . Only the nonzero modes are relevant. There are  $N + 1$  nonzero modes that we label by  $k = 1, 2, \dots, N + 1$ . Here  $0 = \varepsilon_0 < \varepsilon_1 < \varepsilon_2 \dots$ .

The two degenerate ground states for the Hamiltonian  $H_e$  belong to the sectors  $(-1, -1)$  and  $(1, 1)$  [28]. Here we consider the ground state of  $H_e$  belonging to the sector  $(-1, -1)$ , as described by

$$\sigma_0^{(1)}|\Psi_0\rangle = \sigma_{N+1}^{(1)}|\Psi_0\rangle = -|\Psi_0\rangle. \quad (13)$$

It is shown in Ref. [28] that for the Hamiltonian  $H$  with  $h_L > 0$  and  $h_R < 0$ , the ground state and first excited state are the first and second excited states of  $H_e$ , respectively. They belong to sector  $(1, -1)$  and are given by

$$|\Psi_1\rangle = \eta_1^\dagger|\Psi_0\rangle, \quad |\Psi_2\rangle = \eta_2^\dagger|\Psi_0\rangle. \quad (14)$$

The energy gap is given by the difference between the energies of these two states:

$$\Delta = \varepsilon_2 - \varepsilon_1. \quad (15)$$

For  $h_L > 0$  and  $h_R < 0$ , the boundary magnetization of  $\sigma_1$  for the ground state is given by (see Appendix B)

$$m_1 = \langle\Psi_1|\sigma_1|\Psi_1\rangle = \frac{1}{2|h_L|s_0} \left[ -\varepsilon_1\psi_{1,0}^2 + \sum_{k=2}^{N+1} \varepsilon_k\psi_{k,0}^2 \right]. \quad (16)$$

Generally, the couplings  $K_i$  can be arbitrary. If  $K_i$  are random, it is just the model with random bonds.

Because we discuss the order states, the parameter  $g$  are always  $g < 1$ . In our previous work we have studied the quantum wetting transition on a clean lattice with uniform interaction, i.e.,  $K_i = K$  for all sites [33]. For  $h_L h_R < 0$  and  $|h_R|, |h_L| < \sqrt{1-g}$ , there is a first-order phase transition at  $h_L = -h_R$ . In this phase transition, the competition between the two boundaries is the cause of the phase transition. For  $|h_R| > \sqrt{1-g}$ , there a second-order phase transition at  $|h_L| = \sqrt{1-g}$  provided that  $h_L h_R < 0$ . Or vice versa.

Throughout the paper we set  $h_R = -1$  to keep the magnetization negative at the right side of the Ising chain and avoid the phase transition caused by the competition between the two boundaries (mentioned above), in which the random bonds in

the lattice play no role. We set  $h_L > 0$  to study the quantum wetting transition.

A classical critical wetting transition is said to occur if at  $h = 0^-$  the thickness of the layer with positive magnetization diverges continuously as the temperature  $T$  (or, equivalently, surface field  $h$ ) approaches some wetting temperature  $T_w$  (surface field  $h_w$ ) from below [21]. In the quantum wetting transition, both  $g$  and  $h_L$  can control the transition since the transition point depends on both  $g$  and  $h_L$  [see Eq. (25) in the next section]. To be simple, we fix  $g$  and change  $h_L$ . Of course one can fix  $h_L$  and change  $g$ . The results are qualitatively the same.

### III. PHASE TRANSITION WITH ONE DEFECT

First, we solve the solution with one defect. Consider an infinitely long Ising chain with couplings  $K_{N_1} = \zeta$ ,  $K_i = 1$  for  $i \neq N_1$ . The defect bond lies between sites  $N_1$  and  $N_1 + 1$ .

There are two types of eigenvectors for the matrix  $\mathbf{C}$ : extended states and localized states. Both types of eigenvectors can be generally given by  $ae^{ikj} + be^{-ikj}$  for site  $j$  away from the boundaries and the defect. The corresponding eigenvalue is given by  $\varepsilon^2(k) = 4[1 + g^2 - g(e^{ik} + e^{-ik})]$ . For real  $k$ , the eigenvectors are extended. For imaginary  $k = ik_1$ , the eigenvectors are localized. Usually we let  $x = e^{k_1}$  in the localized state eigenvectors. We only consider the localized state eigenvectors of the matrix  $\mathbf{C}$ . These eigenvectors are given by

$$\begin{aligned} \psi_{k,0} &= (-1)^{N_1}(\alpha u + \beta v x^{-N_1})/h_L, \\ \psi_{k,j} &= (-1)^{N_1-j}(\alpha u x^{-j} + \beta v x^{j-N_1}), \quad 1 \leq j \leq N_1, \\ \psi_{k,j} &= (-1)^{j-N_1-1} \beta x^{N_1+1-j}, \quad j > N_1, \end{aligned} \quad (17)$$

where  $k = 1, 2$  label the possible eigenvectors. Additionally, we consider the infinitely long chain to simplify the solution. If the Ising chain is finite, there should be a reflected wave from the right end for  $j > N_1$  in the above equation [34]. Since the chain is infinitely long, the reflected wave vanishes. Obviously it should have  $x > 1$  to guarantee that the state is localized at the left end or the defect. Otherwise, the eigenvector  $\psi_{k,j} = (-1)^{j-N_1-1} \beta x^{N_1+1-j}$ ,  $j > N_1$  goes to infinity for  $j \rightarrow \infty$ . The parameters  $\alpha$  and  $\beta$  are defined by

$$\alpha = \frac{h_L \sqrt{x_L^2 - 1}}{\sqrt{x_L(x_L - g)}}, \quad \beta = \frac{\sqrt{x_+^2 - 1}}{\sqrt{x_+^2 + \zeta^2}}, \quad (18)$$

where

$$x_L = \frac{1 - h_L^2}{g} \quad (19)$$

and

$$x_{\pm} = \frac{1}{2g} [1 - \zeta^2 \pm \sqrt{(1 - \zeta^2)^2 + 4g^2 \zeta^2}]. \quad (20)$$

The eigenvalues of these eigenvectors satisfy

$$\varepsilon^2(x) = 4[1 + g^2 - g(x + x^{-1})]. \quad (21)$$

It should be pointed out that the localized states has lower energies than any extended state since their eigenvalues are given by  $\varepsilon^2 = 4[1 + g^2 - 2g \cos q]$ , where  $q$  are the wave

vectors of the extended states, considering  $x + x^{-1} > 2$  for  $x > 1$ .

By substituting into Eq. (10), we obtain

$$(x - x_L)u + \delta_1 v = 0, \quad \delta_2 u + (x - x_+)v = 0, \quad (22)$$

where

$$\delta_1 = \frac{xh_L^2(x - x^{-1})\beta}{(g - x)\alpha} x^{-N_1}, \quad (23)$$

$$\delta_2 = \frac{(1 - \zeta^2)(g - x)\alpha}{g(x_+ - x_-)\beta} x^{-N_1}. \quad (24)$$

For  $N_1 \rightarrow \infty$ , it has  $\delta_1 = \delta_2 = 0$ . Then Eq. (22) has two solutions:  $x = x_+$  or  $x = x_L$ . The former solution is localized at the defect and the latter one at the left boundary.

Since the solution is localized, it requires  $x_+, x_L > 1$ . We get  $h_L < \sqrt{1 - g}$  and  $\zeta < 1$  by considering Eqs. (19) and (20). In addition, wetting transition requires that  $0 < h_L$ , and the ferromagnetic Ising model which we consider means  $0 < \zeta$ . Putting them together, we get the parameter domain  $0 < h_L < \sqrt{1 - g}$  and  $0 < \zeta < 1$ .

The phase transition occurs at  $x_L = x_+$  where the two roots in the above equations are degenerate. Thus, the surface field at the transition point is given by

$$h_w = \left\{ \frac{1}{2}[(1 + \zeta^2) - \sqrt{(1 - \zeta^2)^2 + 4g^2\zeta^2}] \right\}^{1/2}. \quad (25)$$

For a chain with size  $N_1 \gg 1$  in the scaling region  $|h_L - h_w| \ll 1$ , in Eq. (22), we have

$$\delta_1 \approx \delta_2 \approx \delta = \frac{h_L \sqrt{(x_L^2 - 1)(1 - \zeta^2)}}{\sqrt{g(x_+ - x_-)}} x_L^{-N_1}. \quad (26)$$

In Appendix A it is proved that  $\delta_1 = \delta_2$  at  $h_L = h_w$ .

Since  $x_L > 1$ ,  $\delta$  decays exponentially with the system size  $N_1$ . In the case of  $\delta \ll 1$ , Eq. (22) yields two real roots:

$$x_{1,2} = \frac{1}{2}[(x_L + x_+) \mp \sqrt{(x_L - x_+)^2 + 4\delta^2}]. \quad (27)$$

Substituting them into Eq. (21) yields the energies  $\varepsilon_1$  and  $\varepsilon_2$  of the two lowest states:

$$\varepsilon_{1,2} = 2\sqrt{1 + g^2 - g(x_{1,2} + x_{1,2}^{-1})}. \quad (28)$$

It should have  $x_1 < x_2$  to get  $\varepsilon_1 < \varepsilon_2$ .

Here we discuss the physical picture of this first-order phase transition simply. In the limit of  $N_1 \rightarrow \infty$ , it has  $\delta_1 = \delta_2 = 0$ . Then we have  $x_1 = x_L$ ,  $x_2 = x_+$  and  $\varepsilon_1 = \min[\varepsilon(x_1), \varepsilon(x_2)]$ ,  $\varepsilon_2 = \max[\varepsilon(x_1), \varepsilon(x_2)]$ , where  $\varepsilon(x)$  is defined in Eq. (21). For  $h_L < h_w$ , it has  $\varepsilon_1 = \varepsilon(x_L)$ ,  $\varepsilon_2 = \varepsilon(x_+)$ ; while for  $h_L > h_w$ , it has  $\varepsilon_1 = \varepsilon(x_+)$ ,  $\varepsilon_2 = \varepsilon(x_L)$ . This crossing is the general feature of the first-order quantum phase transition. As the surface field  $h_L$  increases from  $h_L < h_w$  to  $h_L > h_w$ , the ground state changes from that localized at the left end to that at the defect. It should be noted that the eigenvalue of the state localized at the defect  $\varepsilon(x_+)$  is independent of the surface field  $h_L$  while  $\varepsilon(x_L)$ , which is the eigenvalue of the state localized at the left end, depends on  $h_L$ .

From  $\Delta = \varepsilon_2 - \varepsilon_1$  we obtain the scaling relation for the energy gap:

$$\Delta = \Delta_0 \sqrt{1 + \kappa^2}, \quad (29)$$

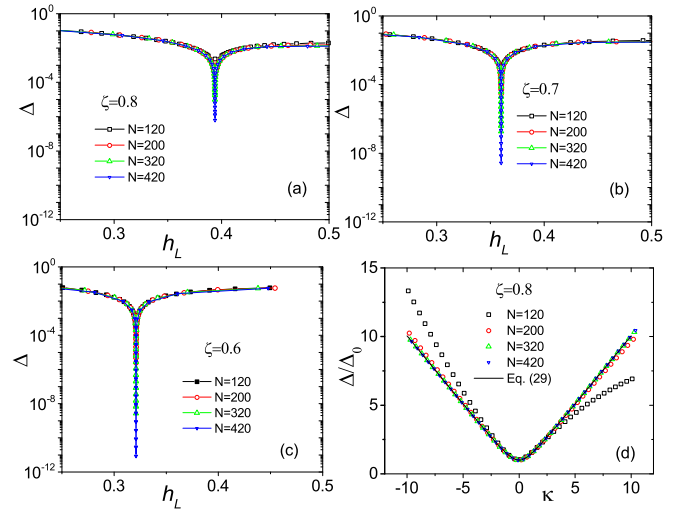


FIG. 1. Energy gaps around the first-order phase transition with  $\xi = 0.6, 0.7, 0.8$ . The transverse field is set to be  $g = 0.8$ . The defect position is set to be  $N_1 = N/2$ . The parameter  $\kappa$  is defined in Eq. (30).

where

$$\Delta_0 = \frac{4g(1 - x_+^{-2})\delta}{\varepsilon_w}, \quad \kappa = \frac{(h_L - h_w)}{\delta_h}. \quad (30)$$

$\kappa$  is the scaling variable and

$$\varepsilon_w = 2\sqrt{1 + g^2 - g(x_+ + x_+^{-1})}, \quad \delta_h = g\delta/h_w. \quad (31)$$

We test this scaling relation with the numerical solution of eigenvalues. Figures 1(a)–1(c) show the energy gaps versus  $h_L$  with various lattice sizes for  $\zeta = 0.6, 0.7, 0.8$ . In the numerical solutions, we cannot let the lattice be infinity. Instead, we carry out the calculation on lattices with  $N = 120, 200, 320, 420$  and set  $N_1 = N/2$ . The right boundary must cause some effects not predicted in the above exact solution on an infinitely long lattice. We expect that the distance from the defect to the right boundary is far enough so that the effects of the right boundary can be neglected. Our numerical results on large size lattices indeed agree with the exact solution on the infinitely long lattice.

From Eq. (25) one can obtain  $h_w = 0.32111025\dots, 0.36010398\dots, 0.39391521\dots$  for  $\zeta = 0.6, 0.7, 0.8$ . The minimum of the gaps are just at these positions. The data collapse on the above scaling relation (29) for  $\zeta = 0.8$  is shown in Fig. 1(d). The scaled data for  $N = 120$  obviously deviate from the scaling relation due to the finite-size effect, while for  $N = 200, 320, 420$ , the data collapse on the scaling relation (29) very well.

The scaling relation (29) is in agreement with the two lowest energy states ansatz for the first-order quantum phase transition proposed by Campostrini *et al.* [35]. Moreover, it is solved exactly in this model.

There is a jump at the transition point for the surface magnetization, as shown in Figs. 2(a)–2(c). To study the jump of the boundary magnetization, as shown in Figs. 2(a)–2(c), we define the singular boundary magnetization:

$$m_{1s} = m_1(h_L) - m_{10}, \quad (32)$$



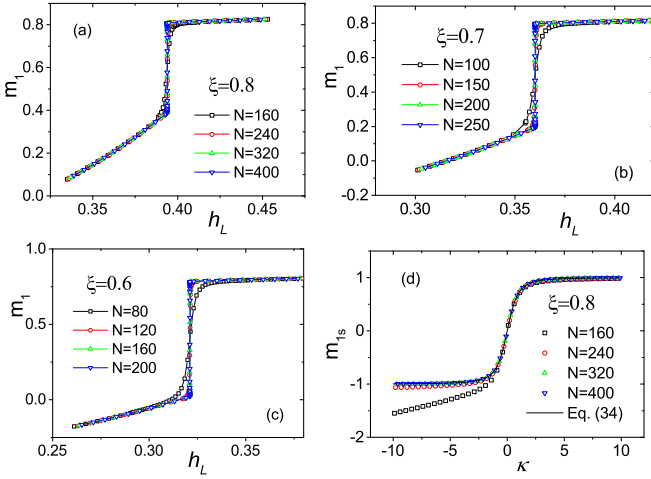


FIG. 2. Surface magnetization  $m_1$  around the first-order phase transition with  $\xi = 0.6, 0.7, 0.8$ . The transverse field is set to be  $g = 0.8$ . The parameter  $\kappa$  is defined in Eq. (30).

where  $m_{10}$  is the boundary magnetization at the transition point, i.e.,

$$m_{10} = m_1(h_L)|_{h_L=h_w}. \quad (33)$$

The transition point  $h_L = h_w$  is the midpoint of the jump, as shown in Fig. 2(c). In the scaling region in which the jump occurs approaches zero in the limit of  $N \rightarrow \infty$ , the variations in the extended state eigenvectors approach zero. Then, the contribution from the extended states can be ignored so that the singular boundary magnetization is given by

$$m_{1s} \approx \frac{1}{2h_{Ls0}} (-\varepsilon_1 \psi_{1,0}^2 + \varepsilon_2 \psi_{2,0}^2) = \Delta_{m1} \frac{\kappa}{\sqrt{1+\kappa^2}}, \quad (34)$$

where the boundary magnetization jump amplitude is given by

$$\Delta_{m1} = \frac{\varepsilon_w (x_+^2 - 1)}{2h_w (x_+^2 + h_w^2 - 1)}. \quad (35)$$

Figure 2(d) shows the FSS of the singular boundary magnetization for  $\zeta = 0.8$ . For  $N = 160$ , the scaling data deviate from the scaling relation (34), while for  $n = 200, 320, 420$ , the scaled data collapse on the scaling relation (34) very well.

The magnetization profiles can provide more information about the phase transition. In Fig. 3 we show four typical magnetization profiles for  $\zeta = 0.6$  and  $N = 200$ , and the defect is at the middle of the chain.

As shown in Fig. 3, the interface across which the magnetization sign changes is localized at the left end of the chain for  $h_L < h_w$ , while the interface is localized at the defect. At the transition point  $h_L = h_w$ , the interface jumps from the left end of the chain to the middle of the chain, where the defect is located. This is additional evidence that the phase transition is of first order.

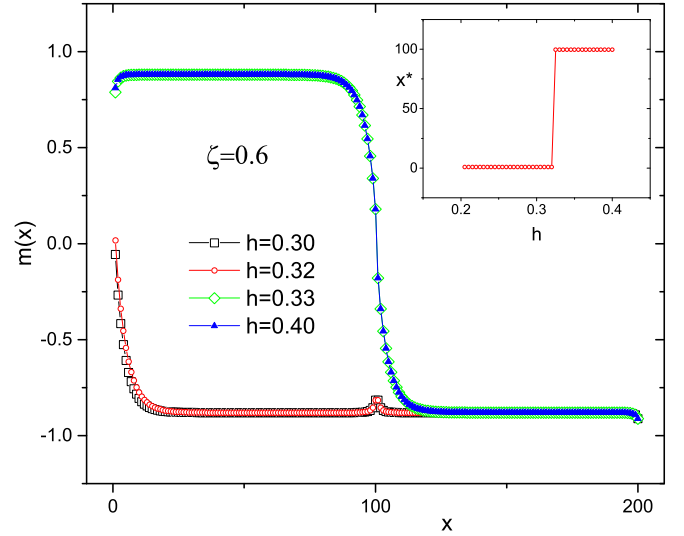


FIG. 3. Magnetization profiles below and above the transition point  $h_w = 0.32111 \dots$ . The transverse field is set to be  $g = 0.8$ . The inset shows the interface position vs the surface field.

#### IV. PHASE TRANSITION WITH TWO DEFECTS

If two defects exist in the Ising chain, what happens to the phase transition? We solve the model numerically with the method we developed previously [34].

We consider two cases with  $N = 200$ . In the first case we set  $J_{80} = \zeta_1 = 0.6$ ,  $J_{120} = \zeta_2 = 0.7$ , with one defect bond between the 80th and 81th sites and another defect bond between the 120th and 121th sites. In the second case we swap the positions of the two defect bonds and set  $J_{80} = 0.7$ ,  $J_{120} = 0.6$ .

From the plots of the energy gap vs surface field  $h_L$  in Fig. 4(a), we can see that the phase transition occurs at

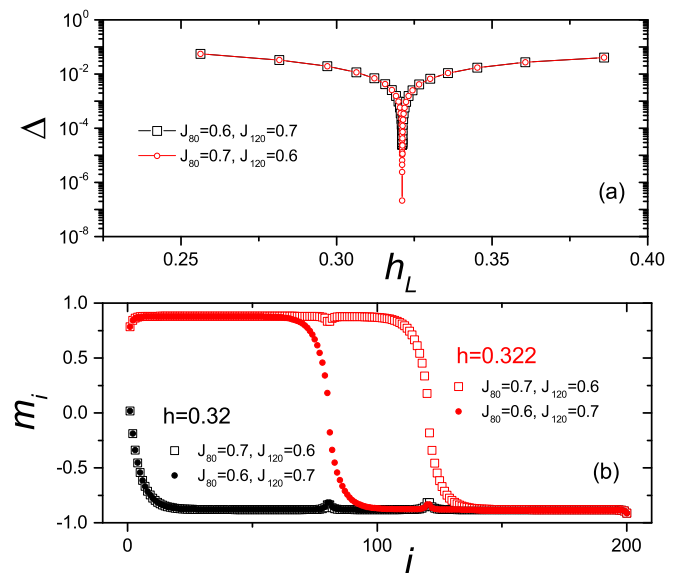


FIG. 4. (a) The energy gap around the first-order phase transition with two defects. The transverse field is set to be  $g = 0.8$ . (b) Typical magnetization profiles above and below the wetting transition point  $h_w$ .

approximately  $h = 0.321$  for the two cases. This transition point is just  $h_w = 0.32112025\dots$  for  $\zeta = 0.6$  in the one-defect case. Therefore, we can guess that the phase transition is determined by the defect of  $J = 0.6$  rather than that of  $J = 0.7$ . This conjecture is further proven by the magnetization profiles for the cases with two defects shown in Fig. 4(b). For surface field below the transition point  $h_L < h_w = 0.3211$ , the interfaces are localized at the left end of the chain. Above the transition point  $h_L > h_w$ , the interface jumps to the defect with  $J = 0.6$ , which is located at  $n = 80$  for the first case and  $n = 120$  for the second case. The phase transition is dominated by the weaker defect because the mode localized at the weaker bond has lower energy.

Enlightened by the phase transition with one defect in the above section, the effects of two defects can be understood in general. Assume the two defect bonds with  $J = \zeta_1, \zeta_2$  are far away from each other and also far away from the left end, there should be three states localized at the left end and the two defects, respectively. Their eigenvalues are given by  $\varepsilon(x_L)$ ,  $\varepsilon(x_{1+})$ , and  $\varepsilon(x_{2+})$ , respectively, where  $x_L = (1 - h_L^2)/g$  and  $x_{1+,2+} = [(1 - \zeta_{1,2}^2 + \sqrt{(1 - \zeta_{1,2}^2)^2 + 4g^2\zeta_{1,2}^2})/(2g)]$  [see Eq. (20)]. Obviously  $\varepsilon(x_{1+})$  and  $\varepsilon(x_{2+})$  are independent of  $h_L$ . The eigenvalue  $\varepsilon(x_L)$  increases with  $h_L$ . The phase transition takes place at  $\varepsilon(x_L) = \min[\varepsilon(x_{1+}), \varepsilon(x_{2+})]$  from which we can get the transition point  $h_w$ . Since  $x_+$  increases with  $\zeta$ , the weaker bond with smaller  $J$  leads to a localized state with smaller eigenvalue. Approximately for  $h_L < h_w$  the state localized at the left end is the ground state and for  $h_L > h_w$  the state localized at the defect with smaller eigenvalue is the ground state. Therefore the defect with weaker bond dominates the phase transition.

## V. FINITE-SIZE EFFECTS IN RANDOM BOND CASES

We consider the iteration in the following form:

$$K_i = 1 + \delta K_i \quad (36)$$

and  $\delta K_i$  has the rectangular distribution

$$P(\delta K) = \begin{cases} 1/w, & -w/2 < \delta K < w/2, \\ 0, & \text{otherwise.} \end{cases} \quad (37)$$

Anderson's localization theory tells us that all the wave functions in the one-dimensional disordered system are localized [36,37]. In the present model, the eigenstate of matrix C defined in Eq. (10) with the lowest energy determines the phase. All the eigenstate of matrix C should be localized due to the random bonds as long as the lattice length is much longer than the localization length. We study the distribution with  $w = 0.2$  as a typical case. In the numerical calculations, we set  $g = 0.8, w = 0.2$  and investigate the samples with lattice size from  $N = 100$  to  $N = 350$ . The strength of the disorder is strong enough to cause the localization length to be much shorter than the lattice size. It is expected that the distribution of the disorder will not affect the qualitative properties of the phase transition as long as the disorder strength is strong enough and the lattice sizes are large enough.

Before discussing the statistical properties of the phase transition, we investigate the finite-size effects from some typical samples. In Fig. 5 we show the plots of the energy

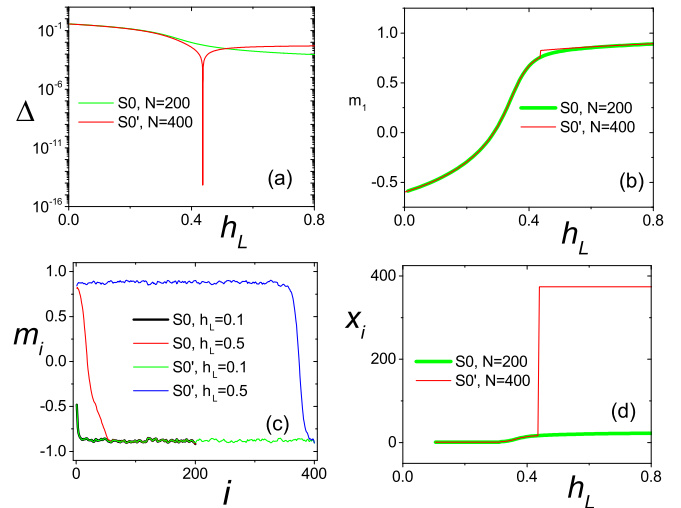


FIG. 5. (a) The energy gap for a typical sample and its lengthened version. (b) Magnetization vs surface field for these two samples. (c) Magnetization profiles at low and high surface fields for these two samples. (d) Interface positions vs surface field for these two samples.

gap, surface magnetization, and the interface position vs the surface field for two samples, which we call S0 and S0'. The size of sample S0 is  $N = 200$ , the size of sample S0' is  $N = 400$ , and the bonds  $J_i$  for  $0 < i < 200$  are the same for the two cases. In other words, sample S0' is sample S0 added to another chain with 200 random bonds.

In Fig. 5(a) one can see that there is no gap closing for sample S0, while there is an obvious gap closing for sample S0'. This indicates that there is no wetting transition for sample S0, whereas there is for S0'. In Fig. 5(b) the surface magnetization shows this point further. There is no jump in the surface magnetization for sample S0, while there is a jump at  $h_L = 0.437$  for sample S0'. In Fig. 5(c) we show the magnetization profiles at two surface fields  $h_L = 0.1, 0.5$  for samples S0 and S0'. In Fig. 5(d) the plot of interface position vs surface field shows that the interface changes continuously for sample S0 and discontinuously for S0'.

This is the first finite-size effect of this model: For a small lattice, there may be no wetting transition. For a lengthened lattice, a wetting transition appears.

As the lattice is lengthened in this way, are there other ways to change the wetting transition? There are three ways in addition to that discussed above.

We present three groups of samples: S1 and S1'; S2 and S2'; and S3 and S3'. The relation between S1, S2, S3, and S1', S2', S3' is the same as that between S0 and S0'. The size of samples S1, S2, and S3 is  $N = 200$ ; the size of samples S1', S2', and S3' is  $N = 400$ ; and the bonds  $J_i$  for  $0 < i < 200$  are the same for these three groups. In other words, sample S1' is sample S1 added to another chain with 200 random bonds, and so on. In Figs. 6, 7, and 8 we compare these three groups of samples.

The first way to change the wetting transition is that the phase transition occurs at a new point. Samples S1 and S1' belong to this case. The transition point is  $h_w = 0.3341569$  for sample S1 and  $h_w = 0.3268872$  for sample S1'. The energy

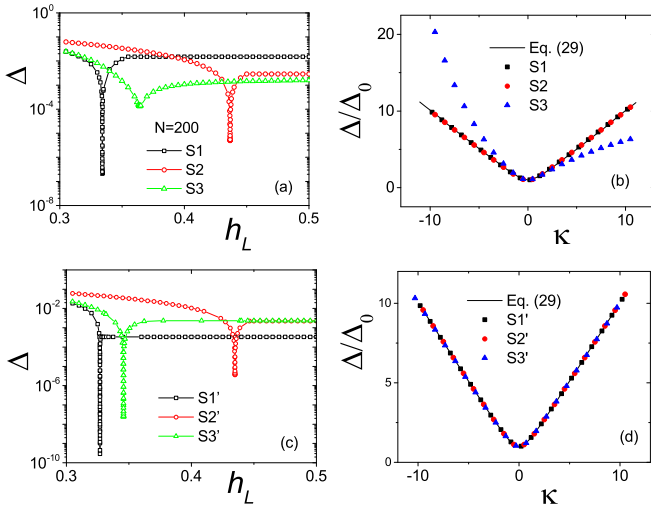


FIG. 6. (a) Energy gap vs surface field  $h_L$  for samples S1, S2, and S3. (b) The energy gap rescaled by Eq. (29) for samples S1, S2, and S3. (c) Energy gap vs surface field  $h_L$  for samples S1', S2', and S3'. (d) The energy gap rescaled by Eq. (29) for samples S1', S2', and S3'. The parameter  $\kappa$  is defined in Eq. (30).

gaps are much different also. The minimal energy gap is  $\Delta_0 = 2.16 \times 10^{-7}$  for sample S1 and  $\Delta_0 = 5.32 \times 10^{-11}$  for sample S1'. The parameter  $\delta_h = 2.71 \times 10^{-7}$ ,  $6.49 \times 10^{-11}$  for samples S1 and S1' respectively.

The second way is that the phase transition point and energy gap vary little. Samples S2 and S2' belong to this type. The transition point is  $h_w = 0.4366918$  for sample S2 and  $h_w = 0.4347999$  for sample S2'. The energy gap is  $\Delta_0 = 5.08 \times 10^{-6}$  and  $\Delta_0 = 3.69 \times 10^{-6}$ . The parameter  $\delta_h = 2.00 \times 10^{-5}$ ,  $1.42 \times 10^{-5}$  for samples S2 and S2', respectively.

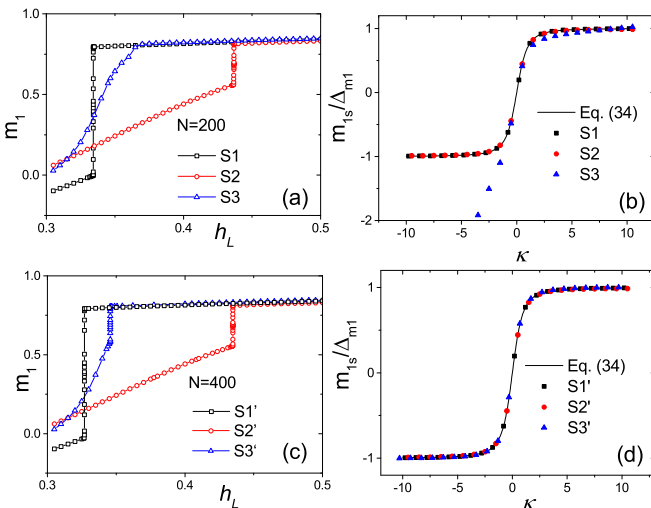


FIG. 7. (a) The surface magnetization vs surface field  $h_L$  for samples S1, S2, and S3. (b) The surface magnetization rescaled by Eq. (34) for samples S1, S2, and S3. (c) The surface magnetization vs surface field  $h_L$  for samples S1', S2', and S3'. (d) The surface magnetization rescaled by Eq. (34) for samples S1', S2', and S3'. The parameter  $\kappa$  is defined in Eq. (30).

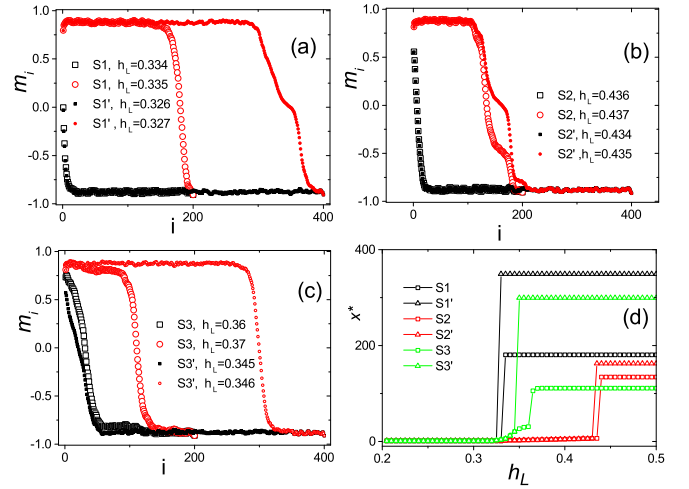


FIG. 8. (a)–(c) The magnetization profiles for three groups of samples below and above the transition point. (d) Interface position vs surface field for the three groups of samples.

The last way is that the phase transition is not remarkable for the short chain, and a remarkable phase transition appears in the lengthened chain. Samples S3 and S3' belong to this case. The transition point is  $h_w = 0.3642699$  for sample S3 and  $h_w = 0.3456786$  for sample S3'. The minimal energy gap is  $\Delta_0 = 2.13 \times 10^{-3}$  for sample S3 and  $\Delta_0 = 1.06 \times 10^{-7}$  for sample S3'. The parameter  $\delta_h = 2.13 \times 10^{-3}$ ,  $1.06 \times 10^{-7}$  for samples S3 and S3', respectively.

We rescaled the data with scaling relation Eq. (29), where the parameters  $\Delta_0$  and  $\delta_h$  are fitted from the data. The rescaled data for samples S1, S2, and S3 are shown in Fig. 6(b). The data collapse on the scaling relation Eq. (29) for samples S1 and S2 but not for S3. Therefore, it can be said that the phase transition for sample S3 is not obvious. The rescaled data for samples S1', S2', and S3' all collapse on the scaling relation Eq. (29), which is the scaling relation of the first-order quantum phase transition [34].

In Fig. 7 we show the surface magnetization for the three groups of samples. More features of the phase transition can be seen in this figure. Figure 7(a) shows samples S1, S2, and S3. The surface magnetization has a remarkable jump for samples S1 and S2. In contrast, the jump is not obvious for sample S3. Moreover, we rescaled the data with scaling relation Eq. (34), where the parameters  $\Delta_{m1}$  and  $\delta_h$  are fitted from the data. In Fig. 7(b) we found that the data can collapse for samples S1 and S2 but not for S3. Figure 7(c) shows the lengthened samples S1', S2', and S3'. The jump in the surface magnetization is obvious for the three samples. We rescaled the data with scaling relation Eq. (34) similarly in Fig. 7(d) and found that the data can collapse for all the samples S1', S2', and S3'.

A physical picture of these three ways of changing as the chain is lengthened can be seen by comparing the magnetization profiles. In Fig. 8 we show the magnetization profiles above and below the phase transition point for the three groups of samples.

From the magnetization profile we can obtain the position  $x^*$  of the interface (or domain wall, where the magnetization

is zero). If  $m_j > 0$  and  $m_{j+1} < 0$ , the magnetization changes sign, we obtain  $x^*$  by a simple interpolation

$$x^* = j + \frac{m_j}{m_j - m_{j+1}}. \quad (38)$$

In Fig. 8(a) the magnetization profiles for samples S1 and S1' are compared. For sample S1, at  $h_L = 0.335$ , which is above the transition point  $h_w = 0.3341569$ , the interface is localized at  $x^* \approx 180$ . For sample S1', at  $h_L = 0.327$ , which is above the transition point  $h_w = 0.3268872$ , the interface is localized at  $x^* \approx 349$ . This infers that as the chain is lengthened, the bonds around  $x^* \approx 349$  are weaker than the bonds around  $x^* \approx 180$ .

In Fig. 8(b) the interface position changes slightly. Above the transition point, the interface position is  $x^* \approx 131$  for sample S2 and  $x^* \approx 159$  for sample S2'. This change should be regarded as a finite size effect since the interface is localized in the original first 200 sites rather than the lengthened part. As mentioned above, the changes in the minimal energy gaps and surface magnetization are not remarkable.

In Fig. 8(c) the interface positions above the transition point are  $x^* \approx 110$  for sample S3 and  $x^* \approx 295$  sample S3'. For sample S3 the surface magnetization does have an obvious jump at the transition point, as shown in Fig. 7(a), while it has an obvious jump for sample S3', as shown in Fig. 7(c).

Figure 8(d) shows the interface position vs the surface field for the three groups of samples. The feature of the first-order phase transition is remarkable. At the transition point, the interface jump from the left end of the chain to somewhere in the middle of the chain.

We summarize the finite-size effects as follows:

(1) For a small lattice, there may not exist a ‘‘phase transition,’’ and the energy gap varies smoothly with the surface field.

(2) As the lattices are lengthened, a phase transition may appear, and the energy gap almost closes.

(3) As a lattice with a phase transition is lengthened, the transition point may change to a new point. At the new transition point, the transition is more singular since the minimal energy gap  $\Delta_0$  is closer to zero, and the interface jump from the left end to the farther position.

(4) The energy gap around the transition point satisfies the scaling relations for the first-order phase transition.

## VI. THE STATISTICAL PROPERTIES FOR THE RANDOM BOND CASES

We study the distributions of transition point  $h_w$  and the minimum energy gap  $\Delta_0$  for different sizes. The random bond distribution is given by Eq. (36).

The procedure to get  $h_w, \Delta_0$  is as follows. At first, we calculate the energy gap at  $h_L = 0.01, 0.02, 0.03, \dots$ . If the energy gap at a point is smaller than those of two neighbored points, we take the two neighbored points as the lower and upper bound of  $h_L$ . The transition usually occurs in this range. Between these two bounds we divide this interval into four equal parts and get five points. Then compare the energy gaps of the middle three points and pick out the one at which the energy gap is minimal. Take this point as the central point and the two neighbored points as the lower and upper bounds.

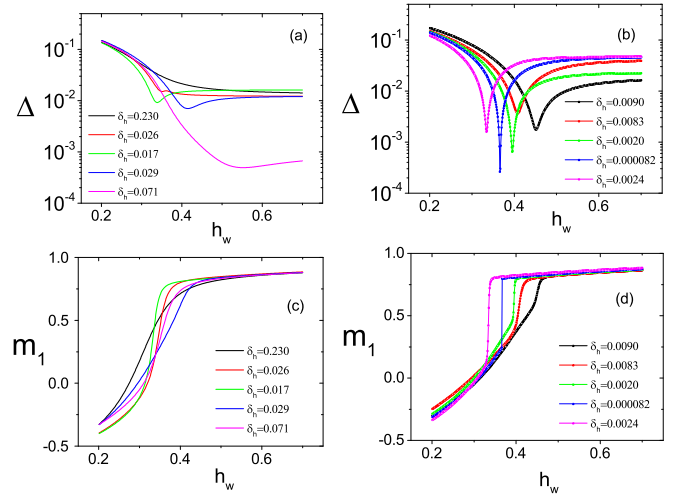


FIG. 9. (a) and (c) The energy gap and surface magnetization for five invalid samples with  $\delta_h > 10^{-2}$ . (b) and (d) The energy gap and surface magnetization for five valid samples with  $\delta_h < 10^{-2}$ . The samples are labeled by their  $\delta_h$ .

We divide this interval into four equal parts and compare the energy gaps of the middle three points. After repeating this procedure many times until the relative differences between the energy gap at the central point and those at the two neighbored points are smaller 2%. In every step, the interval of  $h_L$  shrinks one half. Usually it takes 20–30 steps, so the accuracy of  $h_L$  is about  $10^{-7}$ – $10^{-9}$ . We take the last central point as the phase transition point and get  $h_w, \Delta_0$ .

Near the phase transition point, the energy gap satisfies the scaling relation Eq. (29), from which one gets

$$\delta_h = \frac{|h_L - h_w|}{\sqrt{(\Delta/\Delta_0)^2 - 1}}. \quad (39)$$

We calculate the width of the phase transition  $\delta_h$  by substituting the data at a neighbored point as  $h_L, \Delta$  into the above equation.

As mentioned above, there may be no phase transition on certain lattices. We call these samples invalid. On the contrary, the valid samples show obvious ‘‘sharp closing’’ of the energy gap and ‘‘sharp jump’’ of the surface magnetization at the transition point. The criteria for the ‘‘valid sample’’ is

$$\delta_h < 10^{-2}. \quad (40)$$

Why the criteria is that? It is a conclusion of observing the energy gap and the surface magnetization for some samples. We show ten samples in Fig. 9, where five samples with  $\delta_h > 10^{-2}$  shown in Figs. 9(a) and 9(c) are invalid and five samples with  $\delta_h < 10^{-2}$  shown in Figs. 9(b) and 9(d) are valid. The energy gap for the invalid samples does not have a sharp cusp, while for the valid samples does. The corresponding surface magnetization for the invalid samples does not have a remarkable jump, while for the valid samples does.

We discard those invalid samples. Only the valid samples, the lattices with a phase transition are taken into account. For  $N = 100$ , 30 000 samples are calculated, and 14 478 samples are valid. For  $N = 150, 200, 250, 300, 350$ , 20 000



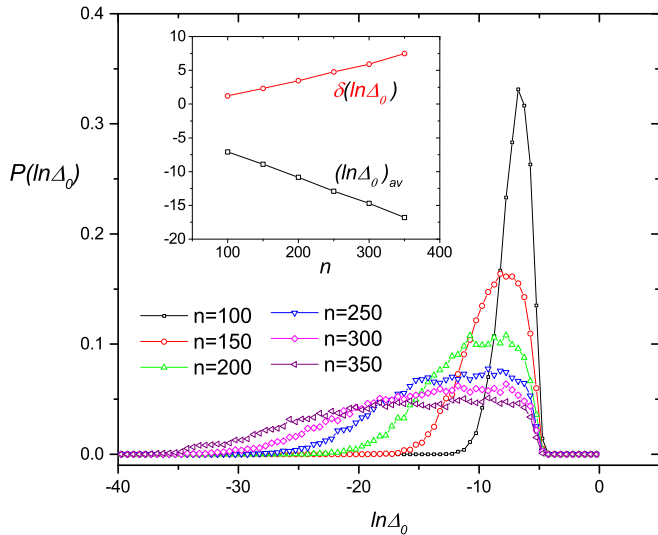


FIG. 10. The distribution of the minimal gap  $\Delta_0$ . The inset shows the average and variation of  $\Delta_0$  for different sizes.

samples are calculated, and the number of valid samples is 13 855, 15 767, 16 503, 17 121, and 17 500, respectively.

We calculate the average of  $\ln \Delta_0$  with  $(\ln \Delta_0)_{av} = \sum_i \ln \Delta_{i0} / n_s$  and the deviation of  $\ln \Delta_0$  with  $\delta(\ln \Delta_0) = \sqrt{\sum_i [\ln \Delta_{i0} - (\ln \Delta_0)_{av}]^2 / n_s}$ . The average and variation in  $\ln \Delta_0$  are shown in the inset in Fig. 10. Their absolute values increase almost linearly with size.

We study the logarithmic distribution of  $\Delta_0$  rather than the distribution of  $\Delta_0$  since the logarithmic of  $\Delta_0$  can show how singular the phase transition is. It is calculated according to

$$P(\ln \Delta_0) = n(x) / n_s \Delta x, \quad (41)$$

where  $n(x)$  is the number of samples satisfying  $x < \ln \Delta_{i0} < x + \Delta x$ , and  $\Delta_{i0}$  is the minimal energy gap for the  $i$ th valid sample. In the numerical calculation we set  $\Delta x = 0.5$ .

Based on the valid sample, we calculate the distribution of the transition point  $h_w$ , defined as

$$P(h_w) = n(h_w) / n_s \Delta h, \quad (42)$$

where  $n_s$  is the number of valid samples,  $n(h_w)$  is the number of samples, for which the transition surface field satisfies  $h_{iw} < h_w < h_{iw} + \Delta h$ , and  $h_{iw}$  is the transition point for the  $i$ th valid sample. In the numerical calculation we set  $\Delta h = 0.01$ . As shown in Fig. 11, the distribution of  $h_w$  varies slightly with the size.

We calculate the average of  $h_w$  and its variation as usual. The average is defined by  $\bar{h}_w = \sum h_{iw} / n_s$ , and the variation of  $h_w$  is defined as  $\delta h_w = \sqrt{\sum_i (h_{iw} - \bar{h}_w)^2 / n_s}$ , where  $h_{iw}$  is the transition point for the  $i$ th sample. For  $N = 100, 150, 200, 250, 300, 350$ , the average  $h_w$  values are given by  $\bar{h}_w = 0.3796, 0.3804, 0.3774, 0.3745, 0.3708, 0.3685$ , respectively. This value decreases with size slowly. The variations in  $h_w$  are shown in the inset in Fig. 11, and  $\delta h_w$  seems to change little.

If one extrapolates this result to the limit of  $N \rightarrow \infty$ , the variation in  $h_w$  should remain finite. This means that the wetting transition point is sample dependent in the

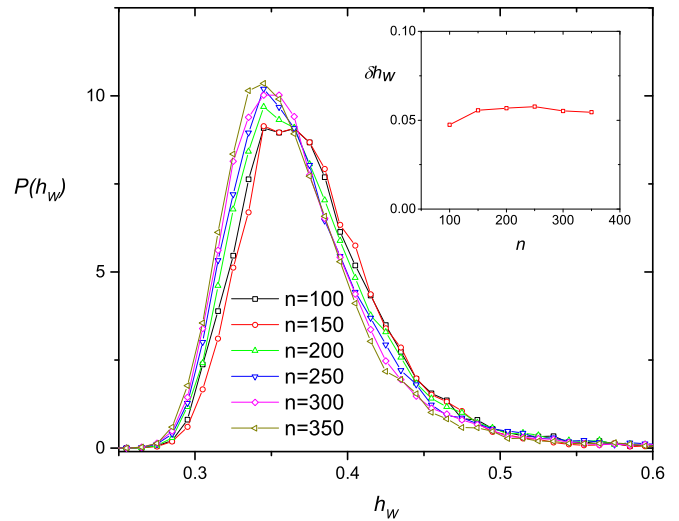


FIG. 11. The distribution of the wetting transition point  $h_w$ . The inset shows the variation of  $h_w$  for different sizes.

thermodynamic limit. This result is strange. We discuss its significance in the last section. We first give an argument for this result.

The discussion in the two-defect case tells us that the wetting transition is determined by the weaker defect. In the random-bond case, there should be many localized states since Anderson's localization theory tells us that all the wave functions in the one-dimensional disordered system are localized [36,37]. The energies of these localized states are not influenced by the surface field  $h_L$  provided the localized regions are far away from the left boundary. Among these localized states, the one with lowest energy should dominate the wetting transition. We denote this state "state II" and the state localized at the left boundary "state I."

We present the  $\varepsilon_1, \varepsilon_2$ , the energies of the ground state and the first excited state for three samples in Fig. 12. The three samples are labeled by their  $\delta_h$ . In fact, these three samples

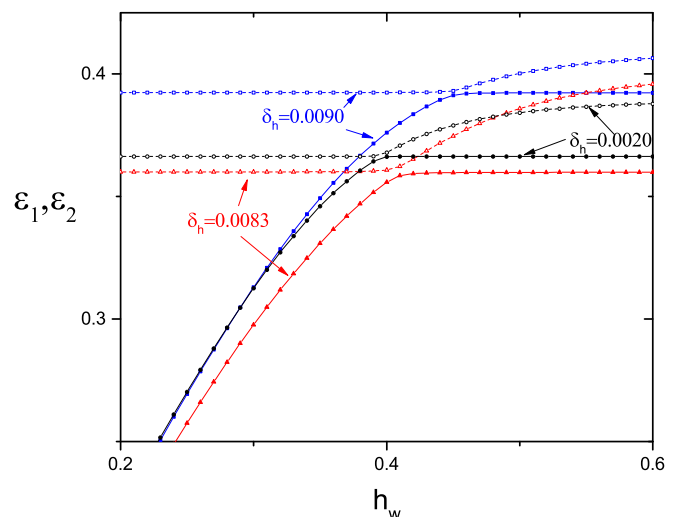


FIG. 12. The energies of the ground state and the first excited state vs the surface field  $h_L$  for three samples.

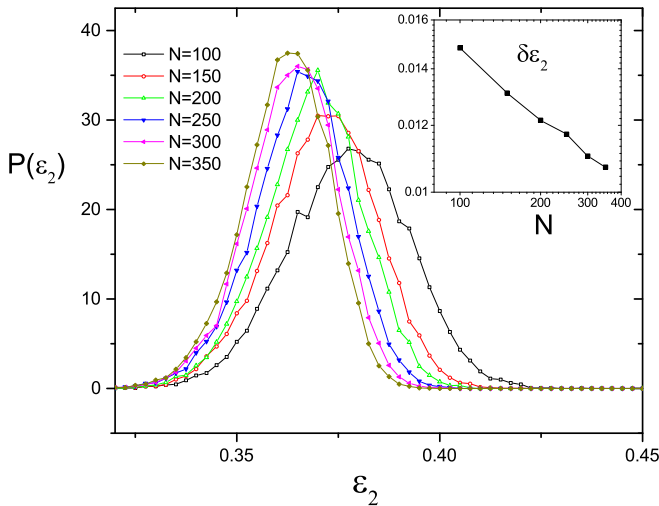


FIG. 13. The probability distributions of the first excited state eigenvalue  $\varepsilon_2$  at  $h_L = 0.2$  for different size lattices. The inset shows the variations of  $\varepsilon_2$  at  $h_L = 0.2$  for different size lattices.

are the same as those in Figs. 9(b) and 9(d). In Fig. 12 one can see that for  $h_L < 0.3$  the ground state energy  $\varepsilon_1$  increases with  $h_L$ , while the excited state energy  $\varepsilon_2$  keeps the same. In fact, the ground state is just state I, which is localized at the left boundary. The first excited state is state II, which is localized in the middle of the lattice. State II is far away from the left end, so its energy do not change as the left surface fields  $h_L$  increase.

The energy of state I, which is localized at the left end, increases with  $h_L$ . As it increases to be equal to that of state II, which is localized in the middle of the lattice, the wetting transition occurs. It is expected that the interface jumps from the left boundary to the region where state II is localized.

See the sample with  $\delta_h = 0.0090$  in Fig. 12. As the energies  $\varepsilon_1, \varepsilon_2$  become equal, the phase transition occurs. As  $h_L$  increases further, state I becomes the excited state and state II becomes the ground state. That is to say,  $\varepsilon_2$  does not change with the surface field  $h_L$  for  $h_L < h_w$  and  $\varepsilon_1$  does not for  $h_L > h_w$ . So are the other samples.

The energy  $\varepsilon_2$  does not change with the surface field  $h_L$  for  $h_L < h_w$ . Obviously it depends on the sample, so we also calculate its distributions for different lattice sizes. Figure 13 shows the distributions of  $\varepsilon_2$  for  $N = 100, 150, 200, 250, 300, 350$ , where  $\varepsilon_2$  is obtained at  $h_L = 0.2$ . From the distribution of  $h_w$  in Fig. 11, one can see that for almost all the samples  $h_w > 0.2$  is satisfied. One can see that the distribution of  $\varepsilon_2$  becomes narrower and higher as the lattice size increases. The inset shows that the deviation of  $\varepsilon_2$  decreases with the lattice size.

The interactions  $K_i$  distribute in a rectangular distribution function  $0.9 < K < 1.1$ . We may call the bond with  $K > 1$  the strong bond and  $K < 1$  the weak bond. Enlightened by the discussion of one defect and two defect cases, we can expect that there are states localized around the weak bonds. The localized state with minimal energy should have many adjacent weak bonds. In the McCoy-Wu model, the groups with a large number of adjacent line defects are the so-called

rare regions [1]. Just the rare regions are responsible for the Griffith-McCoy singularity. We may call the regions with many adjacent weak bonds rare regions. As the system size increases, the maximum of the number of the adjacent weak bonds increases. Then the energy of state localized at the group with most adjacent weaker bonds will converge to the limit of infinite adjacent weakest bonds with  $K = 0.9$ . This limit can be obtained by substituting  $K_i = 0.9$  and  $g = 0.8$  into Eq. (10). It is  $\varepsilon_{\text{limit}} = 0.2$ . As shown in Fig. 13, the distribution of  $\varepsilon_2$  shrinks to the small side. The average of  $\varepsilon_2$  is 0.3786, 0.3724, 0.3700, 0.3668, 0.3648, 0.3633 for  $N = 100, 150, 200, 250, 300, 350$ , respectively. The average of  $\varepsilon_2$  decreases with the lattice size indeed although it is still far from  $\varepsilon_{\text{limit}}$ . The probability of a large number of adjacent weak bonds is exponentially small. Therefore, only on the exponentially large lattice, the average of  $\varepsilon_2$  can approach the limit  $\varepsilon_{\text{limit}}$ .

Consider an infinitely long lattice, the energy of state II approaches  $\varepsilon_{\text{limit}}$ . As the energy of state I grows with  $h_L$ , these two energies intersect at the transition point. As shown in Fig. 12, the growing curves of  $\varepsilon_1$  are different for different samples due to the random bonds. Therefore, even if state II has the same energy  $\varepsilon_{\text{limit}}$ , the intersections with the growing curves of  $\varepsilon_1$  are different. The energy of state I is only related to  $h_L$  and the bonds near the left boundary since state I should be localized and the localization length is finite. State I is localized even if the system is clean. From Eq. (17), for a clean system, we see that the eigenvector of state I is like  $\psi_j \sim x_L^j$ , where  $j$  is the label of the site and  $x_L > 1$ . Its localization length is  $1/\ln x_L$ . From Eq. (19) we know  $x_L = (1 - h_L^2)/g$ . Since the localization length should be shorter if the random bonds are present, we can use  $1/\ln x_L$  to estimate the localization length of state I. From Fig. 11 we can see that most probably the transition point  $h_w < 0.4$ . Letting  $h_L = 0.4, g = 0.8$  in  $x_L = (1 - h_L^2)/g$ , the estimated localization length is about 20. That is to say, on average 20 bonds near the left boundary are related to state I. Therefore, the eigenvalues of state I are fluctuating no matter how large the lattices are. The fluctuation of the eigenvalues of state I is determined by the fluctuation of the 20 bonds near the left boundary.

In the thermodynamic limit  $N \rightarrow \infty$ , on one hand,  $\varepsilon_2$  should approach the limit  $\varepsilon_{\text{limit}}$ , on the other hand,  $\varepsilon_1$  are fluctuating due to the fluctuation of the 20 bonds near the left boundary with the same  $h_L$ . Hence, the transition point  $h_w$ , where  $\varepsilon_1 = \varepsilon_2$ , should be fluctuating from sample to sample even in the thermodynamic limit. The distribution width of  $h_w$  should be finite in the thermodynamic limit.

Figure 10 is easily understood now. As shown in Fig. 10, the distribution of  $\ln \Delta_0$  becomes wider with size. As discussed in the one-defect case, the wetting transition is jumping the interface from the left boundary to the defect. The longer the lattice is, the region with more adjacent weak bonds may exist. Such a region can be anywhere on the lattice, so the distance from the left boundary to this region can be arbitrary. Hence, the minimal energy gap is distributed over a wide range, and the distribution range becomes increasingly wider as the lattice size increases. The minimal energy gap decreases exponentially with the distance from the left boundary to the defect.

VII. SUMMARY

As shown in Fig. 11, the variation of the transition point  $h_w$  changes little as the lattice size increases from  $N = 100$  to  $N = 350$ . For the usual phase transition in disordered systems, the phase transition temperatures converge to a limit as the system size goes to infinity.

One important reason is that the usual phase transition is related to the whole system. As first argued by Brout [38], we may divide the system into  $n$  large subsystems (much larger than the correlation length). If we assume that the coupling between neighboring subsystems is negligible, then the value of any density of an extensive quantity over the whole sample is equal to the average of the (independent) values of this quantity over the subsystems. The pseudo-phase-transition temperature fluctuates from sample to sample due to finite-size effects. However, as the system size goes to infinity, the pseudo-phase-transition temperatures should converge to a limit  $T_C(\infty)$  [39].

In contrast, the present wetting transition is only related to two local parts, the left end and the group of the most adjacent defects, rather than the whole system. Moreover, the present model cannot be divided into two similar subsystems. If the left and right ends are separated, there is no wetting transition. In the McCoy-Wu model, the groups with a large number of adjacent line defects are the so-called rare regions [1]. Near the critical point of the McCoy-Wu model, the rare regions dominate the phase transition [6,7]. In this wetting transition, the situation is more extreme. Only the largest rare region matters.

Moreover, near the left end, the bonds are random, and the effect of the surface field on the left end should be influenced by the bonds near the left end, so the wetting transition point fluctuates with these bonds. Even when the lattice size approaches infinity, this effect does not diminish. Therefore, the wetting transition point should be dependent on the sample in the thermodynamic limit.

ACKNOWLEDGMENTS

The authors thank Prof. Wenan Guo and the SGI in the Department of Physics, Beijing Normal University, for providing computing time.

APPENDIX A: THE SURFACE MAGNETIZATION

We follow Ref. [34] to prove Eq. (16). The surface magnetization  $m_1$  for the ground state is obtained from Eq. (26) with  $\sigma_0^{(1)}\sigma_1^{(1)} = B_0A_1$ , where  $A_i, B_i$  are defined in Eqs. (22) and (23) in [34]. Then  $\sigma_1$  is given by

$$m_1 = \frac{1}{s_0} \left( \psi_{1,0}\phi_{1,1} - \sum_{k=2}^{N+1} \psi_{k,0}\phi_{k,1} \right). \quad (A1)$$

From Eqs. (10) and (12) we get

$$4h_L^2\psi_{k,0} + 4g|h_L|\psi_{k,1} = \epsilon_k^2\psi_{k,0}. \quad (A2)$$

Then we have

$$\psi_{k,1} = \frac{1}{4g|h_L|} (\epsilon_k^2 - 4h_L^2)\psi_{k,0}. \quad (A3)$$

From Eq. (11) we get

$$\phi_{k,1} = \frac{2}{\epsilon_k} (|h_L|\psi_{k,0} - g\psi_{k,1}). \quad (A4)$$

Substituting Eq. (A3) into the above equation yields

$$\phi_{k,1} = -\frac{\epsilon_k}{2|h_L|}\psi_{k,0}. \quad (A5)$$

Substituting it into Eq. (A1) yields Eq. (16)

APPENDIX B: THE EQUALITY OF  $\delta_1$  AND  $\delta_2$  AT THE TRANSITION POINT

We prove Eq. (26). At the transition point it has  $x = x_L = x_+$ , so we let  $x = x_L = x_+$  in Eqs. (23) and (24). Substituting Eqs. (19) and (20) into Eqs. (23) and (24) we get

$$\frac{\delta_1}{\delta_2} = \frac{gx_+^2(x_+ - x_+^{-1})(x_+ - x_-)}{(x_+ - g)(1 - \zeta^2)(x_+^2 + \zeta^2)}. \quad (B1)$$

From Eq. (20) we get

$$x_+x_- = -\zeta^2, \quad x_+ + x_- = \frac{1 - \zeta^2}{g}. \quad (B2)$$

Then we have

$$x_+^2 + \zeta^2 = x_+^2 - x_+x_- = x_+(x_+ - x_-) \quad (B3)$$

and

$$1 - \zeta^2 = g(x_+ - \zeta^2/x_+). \quad (B4)$$

Substituting the above equations into Eq. (B1) yields

$$\frac{\delta_1}{\delta_2} = \frac{x_+^2 - 1}{(x_+^2 - gx_+ - \zeta^2 + g\zeta^2/x_+)}. \quad (B5)$$

From Eq. (B2) we get

$$-\zeta^2 = g(x_+ + x_-) - 1, \quad x_- = -\zeta^2/x_+. \quad (B6)$$

Using the above equations we get that at the transition point

$$\frac{\delta_1}{\delta_2} = \frac{x_+^2 - 1}{(x_+^2 - 1 + gx_- + g\zeta^2/x_+)} = 1. \quad (B7)$$

[1] T. Vojta, *J. Phys. A: Math. Gen.* **39**, R143 (2006).

[2] S. Sachdev, *Quantum Phase Transitions* (Cambridge University Press, Cambridge, 1999).

[3] M. Vojta, *Rep. Prog. Phys.* **66**, 2069 (2003).

[4] C. K. Chiu, J. C. Y. Teo, A. P. Schnyder, and S. Ryu, *Rev. Mod. Phys.* **88**, 035005 (2016).

[5] R. Islam, E. E. Edwards, K. Kim, S. E. Korenblit, C. Noh, H. J. Carmichael, G. D. Lin, L. M. Duan, C. C. J. Wang, J. K. Freericks *et al.*, *Nat. Commun.* **2**, 377 (2011).

[6] D. S. Fisher, *Phys. Rev. Lett.* **69**, 534 (1992).

[7] D. S. Fisher, *Phys. Rev. B* **51**, 6411 (1995).

[8] A. P. Young and H. Rieger, *Phys. Rev. B* **53**, 8486 (1996).

- [9] C. Pich, A. P. Young, H. Rieger, and N. Kawashima, *Phys. Rev. Lett.* **81**, 5916 (1998).
- [10] O. Motrunich, S. C. Mau, D. A. Huse, and D. S. Fisher, *Phys. Rev. B* **61**, 1160 (2000).
- [11] B. M. McCoy and T. T. Wu, *Phys. Rev. Lett.* **21**, 549 (1968).
- [12] B. M. McCoy and T. T. Wu, *Phys. Rev.* **176**, 631 (1968).
- [13] B. M. McCoy, *Phys. Rev. Lett.* **23**, 383 (1969).
- [14] M. Suzuki, *Prog. Theor. Phys.* **56**, 1454 (1976).
- [15] X. T. Wu, *Ann. Phys.* **418**, 168166 (2020).
- [16] M. Aizenman and J. Wehr, *Phys. Rev. Lett.* **62**, 2503 (1989).
- [17] P. G. de Gennes, *Rev. Mod. Phys.* **57**, 827 (1985).
- [18] D. Bonn, J. Eggers, J. O. Indekeu, J. Meunier, and E. Rolley, *Rev. Mod. Phys.* **81**, 739 (2009).
- [19] K. Binder and D. P. Landau, *Phys. Rev. B* **37**, 1745 (1988).
- [20] E. V. Albano and K. Binder, *Phys. Rev. Lett.* **109**, 036101 (2012).
- [21] A. O. Parry, *J. Phys. A: Math. Gen.* **24**, 1335 (1991).
- [22] A. O. Parry, *J. Phys. A: Math. Gen.* **25**, 257 (1992).
- [23] D. B. Abraham, *Phys. Rev. Lett.* **44**, 1165 (1980).
- [24] D. B. Abraham, in *Phase Transition and Critical Phenomena*, edited by C. Domb and J. L. Lebowitz (Academic, London, 1986), Vol. 10, p. 1.
- [25] S. Wiseman and E. Domany, *Phys. Rev. E* **52**, 3469 (1995).
- [26] A. Bellafard and S. Chakravarty, *Phys. Rev. B* **94**, 094408 (2016).
- [27] A. Bellafarda, S. Chakravarty, M. Troyerb, and H. G. Katzgraber, *Ann. Phys.* **357**, 66 (2015).
- [28] M. Campostrini, A. Pelissetto, and E. Vicari, *J. Stat. Mech.* (2015) P11015.
- [29] R. Z. Bariev and I. Peschel, *Phys. Lett. A* **153**, 166 (1991).
- [30] H. Hinrichsen, K. Krebs, and I. Peschel, *Z. Phys. B* **100**, 105 (1996).
- [31] U. Bilstein and B. Wehefritz, *J. Phys. A: Math. Gen.* **32**, 191 (1999).
- [32] E. Lieb, T. Schultz, and D. Mattis, *Ann. Phys.* **16**, 407 (1961).
- [33] K. Hu and X. T. Wu, *Phys. Rev. B* **103**, 024409 (2021).
- [34] If the Ising chain length is finite, say  $N (> N_1)$ , the localized state solution should be  $bx^{N_1+1-j} + b'x^{j-N}$  for  $j > N_1$ , where  $b'x^{j-N}$  is the reflected wave from the right end. As  $N$  goes to infinity, the reflected wave term vanishes.
- [35] M. Campostrini, J. Nespolo, A. Pelissetto, and E. Vicari, *Phys. Rev. Lett.* **113**, 070402 (2014).
- [36] P. W. Anderson, *Phys. Rev.* **109**, 1492 (1958).
- [37] E. Abrahams, P. W. Anderson, D. C. Licciardello, and T. V. Ramakrishnan, *Phys. Rev. Lett.* **42**, 673 (1979).
- [38] R. Brout, *Phys. Rev.* **115**, 824 (1959).
- [39] A. Aharony and A. B. Harris, *Phys. Rev. Lett.* **77**, 3700 (1996).